Published in final edited form as:
*Neuron*. 2011 April 14; 70(1): 82–94. doi:10.1016/j.neuron.2011.02.047.

# Neural Circuit Mechanisms for Pattern Detection and Feature Combination in Olfactory Cortex

**Ian G. Davison**[1] and **Michael D. Ehlers**[1,2,*]

[1] Department of Neurobiology, Duke University Medical Center, Durham, NC 27710, USA

[2] Pfizer Global Research and Development, Neuroscience Research Unit, Groton CT, USA

## Summary

Odors are initially encoded in the brain as a set of distinct physicochemical characteristics, but are ultimately perceived as a unified sensory object – a 'smell'. It remains unclear how chemical features encoded by diverse odorant receptors and segregated glomeruli in the main olfactory bulb (MOB) are assembled into integrated cortical representations. Combining patterned optical microstimulation of MOB with *in vivo* electrophysiological recordings in anterior piriform cortex (PCx), we assessed how cortical neurons decode complex activity patterns distributed across MOB glomeruli. PCx firing was insensitive to single-glomerulus photostimulation. Instead, individual cells reported higher-order combinations of coactive glomeruli resembling odor-evoked sensory maps. Intracellular recordings revealed a corresponding circuit architecture providing each cortical neuron with weak synaptic input from a distinct subpopulation of MOB glomeruli. PCx neurons thus detect specific glomerular ensembles, providing an explicit neural representation of chemical feature combinations that are the hallmark of complex odor stimuli.

## Introduction

Constructing a unified sensory percept from diverse forms of primary receptor input is a challenge faced by all sensory systems, including olfaction (Gottfried, 2010). Among the senses, olfaction is particularly synthetic, as chemical mixtures are commonly perceived as a single unified odor object (Gottfried, 2010; Livermore and Laing, 1996; Wilson and Stevenson, 2003). Synthetic processing is required even for simple monomolecular odorants, whose diverse chemical attributes activate multiple types of peripheral odorant receptors (ORs; Malnic et al., 1999; Wachowiak and Cohen, 2001). Since inputs for each OR type are highly segregated (Mori et al., 1999), the features they encode must be assembled at later processing stages. While unified sensory representations are thought to arise in piriform cortex (PCx), the circuit mechanisms for combining distinct OR inputs remain poorly understood.

Odorants are first represented as a set of physicochemical characteristics, recognized in rodents by a large family of ~1000 ORs. Each olfactory sensory neuron expresses a single



*Corresponding author: Michael D. Ehlers, M.D., Ph.D., Neuroscience Research Unit, Pfizer, Inc., MS 8220-4215, Eastern Point Rd., Groton, CT 06340, USA, Tel: 860.686.3158, FAX: 860.715.8566, michael.ehlers@pfizer.com.

Supplemental Information
Supplemental information contains five figures and Supplemental Experimental Procedures.

OR type determining its chemical selectivity (Bozza et al., 2002; Serizawa et al., 2003), and sensory neurons expressing like ORs send convergent projections to ~2 discrete locations in the main olfactory bulb (MOB) called glomeruli (Mombaerts et al., 1996). The MOB thus encodes chemical information using a topographic map of OR-based sensory channels. Each odor stimulus contains a constellation of chemical attributes that binds multiple ORs, activating distributed, stimulus-specific patterns of MOB glomeruli (Lin et al., 2006; Soucy et al., 2009). Second-order MOB neurons (mitral/tufted cells, or M/Ts) receive direct sensory input from a single OR type, maintaining anatomically separate processing streams. While local circuits modulate second-order odor responses in both rats (Dhawale et al., 2010; Fantana et al., 2008) and insects (Olsen et al., 2007; Olsen and Wilson, 2008; Shang et al., 2007), these lateral interactions also appear to be glomerulus-specific (Fantana et al., 2008; Olsen et al., 2007; Root et al., 2008). The OR map thus organizes the initial routing of chemical information in the MOB, providing the foundation for subsequent odor processing.

Although many key elements of MOB function have been described (Fantana et al., 2008; Mori et al., 1999; Wilson and Mainen, 2006), principles of odor processing in PCx remain unclear. Cortical odor representations are dramatically transformed from the MOB's ordered sensory map. Odors activate widely dispersed neuronal populations lacking apparent spatial organization (Illig and Haberly, 2003; Rennaker et al., 2007; Stettler and Axel, 2009). The stimulus features driving PCx neurons are difficult to identify, due to the complexity and high dimensionality of odor space (Haddad et al., 2008), and the ambiguous mapping between chemical structure and OR binding (Araneda et al., 2000; Katada et al., 2005). Furthermore, most odorants activate multiple ORs, and PCx neurons respond to multiple dissimilar odorants, suggesting they integrate diverse MOB inputs (Apicella et al., 2010; Lei et al., 2006; Wilson, 2000, 2001). Finally, the neural connectivity between MOB to PCx is poorly defined. M/T axons project broadly throughout PCx without obvious patterning (Buonviso et al., 1991; Nagayama et al., 2010; Ojima et al., 1984). Overall, the approaches typically used to describe cortical sensory processing – organized functional maps, single-neuron receptive fields, and anatomically ordered input – have limited usefulness in PCx.

Consequently, the neural computations performed by PCx remain unclear. What are the characteristics of MOB activity that drive firing in PCx neurons? How many MOB glomeruli connect to each PCx cell? How strong are inputs from each glomerulus? *In vitro* data suggest that PCx neurons may respond to relatively few active M/T inputs (Bathellier et al., 2009; Franks and Isaacson, 2005), while *in vivo* results suggest that substantial numbers of glomeruli are required (Arenkiel et al., 2007). Bypassing the complexity of chemical stimuli, we combined patterned optical microstimulation of MOB with electrophysiological recordings in anterior PCx to assess the functional circuit architecture for cortical odor processing. *In vivo* circuit mapping revealed that each PCx neuron sampled a distinct and restricted subpopulation of dispersed MOB glomeruli. While single-glomerulus inputs were weak and ineffective at generating firing, PCx neurons responded reliably when several MOB glomeruli were coactivated in patterns resembling odor-evoked sensory maps. Furthermore, different PCx neurons were sensitive to distinct patterns of MOB output. PCx neurons thus decode MOB activity by detecting higher-order ensembles of coactive glomeruli, providing a circuit basis for neural representation of complex odorants.

## Results

### Targeted Activation of MOB Glomeruli By *In Vivo* Photostimulation

We assessed the neural circuits for odor processing in anterior PCx by measuring cortical responses to systematic activation of MOB glomeruli. Odors are impractical for this purpose, due to the complex relationship between chemical properties and OR activation (Araneda et al., 2000). Many glomeruli are not activated even by large odor sets (Fantana et

al., 2008), and even monomolecular compounds bind multiple OR types (Malnic et al., 1999; Wachowiak and Cohen, 2001). We therefore used *in vivo* scanning photostimulation to focally activate glomeruli in the dorsal MOB of the mouse. UV uncaging of MNI-glutamate (Callaway and Katz, 1993; Shepherd et al., 2003) generated defined MOB output with a resolution similar to natural spacing of glomeruli (Figure 1).

Because PCx receives MOB input via spike trains of M/T neurons (Haberly, 1991), we first characterized uncaging-evoked firing in M/Ts. We recorded extracellular M/T spikes while sequentially photostimulating dorsal MOB locations in a scan pattern composed of an 8 X 12 grid (Figures 1A, 1B, and S1; see Experimental Procedures). Uncaging drove M/Ts with high efficacy, reliably generating spike bursts in >90% of cells at 1-4 MOB sites (Figures 1A-1C; 24/26 M/Ts). Uncaging responses were robust, matching or exceeding the strongest odor responses measured in a parallel set of M/T recordings (Figures 1B and 1D; mean peak firing >100 Hz; median latency <5 ms). Uncaging also provided high spatial resolution. On average, each M/T was driven by only ~2 neighboring MOB sites near the recording electrode (Figures 1E and 1F; mean = 2.2 sites; range 1–4). Recording locations and effective sites were close but non-overlapping, suggesting that M/Ts were driven superficially via their apical dendrites within glomeruli, rather than by somatic activation at deeper layers (Figure S1). Correspondingly, aligning recording locations to the most effective uncaging site revealed a spatial distribution consistent with M/Ts in one or a few activated glomeruli (Figure S1). Because each scan site could potentially overlap with >1 glomerulus in the irregular OR map, we estimated that each site activated ~1–3 glomeruli. Locations outside the primary effective glomerulus did not drive M/T firing (Figures 1F and S1), suggesting lateral excitatory interactions between M/Ts in different glomeruli were either absent or less pronounced than in *Drosophila* (Olsen et al., 2007; Shang et al., 2007). However, our data do not exclude subthreshold effects, inhibition, or other types of interglomerular interactions (Arevian et al., 2008; Dhawale et al., 2010; Fantana et al., 2008; Olsen and Wilson, 2008). Finally, uncaging activated M/Ts within different glomeruli independently (Figure S1). Overall, photostimulation provided targeted, high efficacy manipulation of functionally distinct MOB glomeruli, allowing us to generate highly defined MOB output.

## PCx Neurons are Insensitive to Single-Glomerulus Input

To determine how PCx neurons respond to input from individual MOB sensory channels, we recorded extracellular spikes in PCx while independently photoactivating dorsal MOB glomeruli. PCx neurons exhibited resting activity and were responsive to sensory input, firing readily to odor stimuli (Figures 2A-2D). However, single-site scanning photostimulation of MOB was ineffective at driving action potentials in PCx (Figures 2E-2H). No MOB location tested produced reliable firing in any PCx neuron (32 neurons tested with 96 sites; ≥3 trials/site; Figure S2). The lack of uncaging responses was not due to inadequate M/T activation, as uncaging consistently drove vigorous MOB firing exceeding 100Hz (Figure 2G). On average, uncaging produced MOB firing that exceeded that of even the most effective odorants (Figures 2C and 2G), although our relatively small odorant panel may not have maximally activated M/Ts. The lack of photostimulation responses in PCx was thus in striking contrast to odor-evoked activity. Together, these data suggest that the M/Ts within any single glomerulus provide either no input or at most subthreshold input to each PCx neuron.

## PCx Neurons Respond to Multiglomerular Activity

What accounts for the differences in PCx responses to odors and uncaging? Odors typically drive activation of multiple ORs (Malnic et al., 1999), generating distributed glomerular activity patterns in MOB (Rubin and Katz, 1999; Soucy et al., 2009; Uchida et al., 2000;

Wachowiak and Cohen, 2001). We thus asked whether PCx neurons detect coincident input from multiple glomeruli. Using multisite uncaging to independently control the number and identity of activated glomeruli, we generated naturalistic MOB activity patterns resembling odor-evoked maps (randomly selected patterns of 2–16 sites; see Figure S3 and Experimental Procedures). Successively activating MOB sites 1 ms apart drove temporally overlapping firing of M/Ts at distributed MOB locations, although it may not have fully recreated the temporal patterning characteristic of odor responses (Dhawale et al., 2010). In MOB, the output of individual M/Ts was unaffected by the number of uncaging sites (Figures 3A-3C). In contrast, multisite uncaging revealed that firing began to emerge in PCx when several glomeruli were activated coincidently, and increased as patterns encompassed more glomeruli (Figures 3D-3F). 3-site stimuli were moderately effective, with ~50% of neurons responding to >1 pattern, and most cells responded to several 16-site stimuli (Figures 3G and S3; responses defined as ≥1 spike on ≥1 trial for any pattern). Responses to multisite patterns were comparable to odors for both firing rate and reliability across trials (Figure S3). Averaged across the PCx population, significant firing appeared only for patterns with ≥3–4 uncaging sites (Figure 3F; $p < 0.05$; t-test comparing resting and evoked activity; n = 14–53 neurons for each pattern size). PCx neurons are thus responsive to multiglomerular MOB activity, detecting coincident input from multiple ORs.

Multisite uncaging both generates combinatorial MOB activity and simultaneously increases total cortical input. We tested whether PCx firing depended on the distributed quality of multisite patterns versus their total activity level in two ways. First, we normalized each neuron's firing to the number of uncaging sites in the stimulus pattern. The resulting 'per glomerulus' cortical response was a supralinear function of pattern size, showing a step-like increase for patterns with ≥3–4 sites (Figure 3H). The invariance of M/T firing to the number of uncaging sites (Figures 3A-3C and S3) suggested that supralinearity arose within PCx. Second, we directly compared responses to multisite stimuli and their individual component sites. For a subset of effective 4-site patterns, we also examined firing for each component site activated 4 times at 20 Hz. Although multisite stimuli evoked substantial PCx activity, individual sites produced little or no firing even with repeated stimulation (Figures 3I and 3J). Together, these findings indicate that PCx neurons are strongly sensitive to combinatorial MOB activity patterns resembling those generated by odor stimuli.

## PCx Neurons Detect Specific Glomerular Combinations

We next tested whether PCx neurons discriminated between different glomerular patterns when total cortical input was held constant. We stimulated equal numbers of MOB sites in different configurations, activating distinct subsets of glomeruli to mimic the diverse activity patterns driven by different odorants (Figure 4A; see Experimental Procedures). Varying the identity of active glomeruli often produced markedly different responses in individual PCx cells (Figure 4B). Testing with a series of multisite stimuli revealed pattern-selective firing in many neurons (Figure 4C). Pattern detection by PCx reflected cortical processing rather than differences in potency of our test stimuli, since all patterns were equally effective when averaged across the population sample (Figure S4; $p > 0.2$, Kruskal-Wallis test). We evaluated pattern sensitivity for each cell using a selectivity index (lifetime sparseness, $S_L$) to quantify the extent to which responses were driven solely by a single pattern ($S_L = 1$) versus equally by all patterns ($S_L = 0$). For the majority of neurons, $S_L$ was significantly higher than predicted by a randomly shuffled dataset ($p < 0.05$; Figure 4D; see Experimental Procedures). Pattern selectivity was also consistently higher for measured versus shuffled data at the population level (Figure S4). Single PCx neurons thus appear to detect specific patterns of coactive MOB glomeruli.

Furthermore, we also found that the PCx population collectively detected a wide range of MOB patterns. Different neurons had different response profiles for the same set of

synthetic stimuli (Figure 4C), indicating detection of distinct glomerular combinations. To quantify the diversity in pattern detection across cells, we calculated correlation coefficients for all pairs of response profiles for all neurons, and repeated this analysis for shuffled data. Measured response profiles were consistently more dissimilar than shuffled data (Figures 4E and S4; $p \ll 0.01$ for patterns with 4, 9, and 16 sites; Kolmogorov-Smirnov test; n = 14–39 cells). Taken together, these results demonstrate that the PCx population collectively detects a wide range of possible combinations of MOB glomeruli.

## Direct Synaptic Input to PCx Neurons Has Low Efficacy

The circuit mechanisms supporting glomerular pattern detection by PCx neurons were not apparent from extracellular recordings. We asked whether this computation arose from the circuit architecture mapping MOB output onto individual PCx cells. Each neuron in PCx will decode MOB activity based on the number and identity of glomeruli providing it with direct synaptic input, and on the strength of those inputs. To test network connectivity on this cellular scale, we combined single-site scanning photostimulation of MOB with *in vivo* intracellular recordings of subthreshold synaptic responses in PCx. For each PCx neuron, we classified MOB sites as synaptically connected if they generated time-locked excitatory postsynaptic potentials (EPSPs) that were ≥2 standard deviations above resting membrane potential fluctuations (during a 150 ms analysis window; see Experimental Procedures). Although categorizing EPSPs as mono- or polysynaptic is potentially ambiguous, our data from parallel extracellular experiments showed little or no evoked firing in PCx under the same conditions (Figures 2 and S2). This suggested EPSPs primarily reflected direct MOB input, rather than polysynaptic contributions from recurrent intracortical pathways. While we cannot definitively exclude a polysynaptic component, any additional recurrent input will both increase the size of EPSPs and add to the set of apparently connected glomeruli. Our data therefore represent an upper bound on the effective strength and distribution of connections between the glomerular map in the MOB and neurons in PCx.

We first addressed the strength of single-glomerulus inputs to PCx neurons, measured in the intact olfactory circuit. Photostimulation of any single MOB site generated at most a modest synaptic response, consistent with the lack of spiking seen in extracellular recordings. Despite driving high-frequency spike trains in upstream M/Ts, uncaging generated cortical EPSPs with peak amplitudes between ~0.5–3 mV (Figure 5A). Individual events comprising compound EPSPs could sometimes be resolved, suggesting that input from single M/T spikes was even smaller (Figure 5A, bottom). Plotting the distribution of EPSP sizes for the recorded population confirmed that uncaging responses were consistently weak (Figure 5B). Because responses reflected summed input from trains of M/T spikes, we used integrated EPSP area rather than peak amplitude for further analyses. Overall, our results indicate that the majority of PCx neurons receive relatively weak synaptic input from any single glomerulus, insufficient to drive action potentials.

## Optical Mapping of Olfactory Circuit Connectivity *In Vivo*

Optical microstimulation allowed us to measure the network connectivity that transmits chemical information from the MOB glomerular map to individual PCx neurons. Photostimulation mapping revealed that only a restricted subpopulation of dorsal glomeruli generated detectable EPSPs in each cell (Figures 5C-E; range = 7–11 out of 96 with one outlier of 26, mean = 10.3, n = 8 cells). This limited connectivity reflected the architecture of the olfactory circuit rather than incomplete activation of M/Ts, which uncaging drove with high efficacy. While we cannot rule out additional connections undetected by our recordings, depolarizing synaptic input to PCx neurons was nonetheless heavily weighted towards ~10% of uncaging sites independent of whether they were classified as connected (Figures 5C and 5D). Individual cortical cells thus sample a small fraction of possible

connections with the MOB glomerular array. Some responses were hyperpolarizing, perhaps reflecting local circuit inhibition within PCx (Stokes and Isaacson, 2010), although this was not statistically significant for population data. Overall, we found little consistent evidence for synaptic inhibition with single uncaging sites, which may not have generated firing of PCx interneurons required for feedforward inhibition.

In many sensory systems, topographic ordering of cortical inputs shapes both sensory maps and the receptive fields of single neurons (Reid and Alonso, 1995). We examined whether MOB input to PCx displayed spatial patterning, such as connections from clustered sets of glomeruli or restricted MOB regions. Effective uncaging sites were widely distributed throughout the dorsal MOB without any obvious topographical relationship (Figure 5F). While synaptic input maps of several neurons contained clusters of 2–3 adjacent MOB sites, this was consistent with the resolution of MOB uncaging (~2 uncaging sites per M/T cell), suggesting clustering reflected MOB activation rather than circuit connectivity. Overall, PCx neurons sampled a scattered subset of potential glomerular inputs lacking apparent spatial organization. Furthermore, glomerular input maps for different cortical cells were distinct and largely nonoverlapping (Figure 5F). We evaluated the similarity of glomerular connectivity across neurons by converting input maps for each cell into a vector and calculating a correlation coefficient for all pairwise comparisons. The resulting distribution was heavily biased towards low similarity, suggesting different PCx neurons sampled different glomerular populations (Figure 5G). Together, our intracellular data reveal several principles of cortical odor processing. First, each PCx neuron samples a small and apparently random fraction of potential glomerular inputs. Second, individual connections are relatively weak and have little impact on firing. Third, different PCx cells integrate information from distinct subsets of glomeruli.

## PCx Neurons Respond Cooperatively to Glomerular Combinations

Because odors typically activate multiple OR types, we next compared synaptic input in PCx for single photostimulation sites and multiglomerular stimuli. We first measured odor-evoked EPSPs, which revealed a striking disparity between sensory responses and single-site uncaging. While photostimulation generated EPSPs ~1–3 mV in size, sensory responses could exceed 15–20 mV (Figures 6A and 6B) and were on average ~4–15 times larger than EPSPs from uncaging (for amplitude and integral, respectively; Figure 6C). This ratio was even greater for robust odor responses, indicating that single-glomerulus input is inadequate to account for sensory responses in PCx neurons.

In principle, both large synaptic responses to odors and combination-sensitive firing in PCx could arise from simple summation of weak input from several glomeruli. In other sensory systems, however, distinct input pathways often generate suppressive or supra-additive effects in cortical neurons (Jacob et al., 2008; Usrey et al., 2000). We used multisite uncaging to test for nonlinear interactions between coactive glomeruli, systematically increasing the number of MOB sites while capturing total subthreshold input with intracellular recordings of PCx neurons. Multiglomerular patterns generated robust synaptic responses comparable in size to odor responses (Figures 6D-6F and S5). Averaging EPSPs across the population showed that total input scaled supralinearly with the number of MOB uncaging sites. Synaptic responses to larger patterns were greater than predicted by linear summation of single-site input, which was small but nonzero (Figure 6G). As with extracellular data, we normalized cortical EPSPs to total MOB output by dividing by the number of uncaging sites. Coactivating additional glomeruli led to an increase in the net ‘per glomerulus’ synaptic input as well (Figure 6H). As noted above, supralinearity appeared to emerge in PCx rather than MOB, since M/T firing was independent of uncaging pattern size (Figure S3H-S3L).

Supralinearity could potentially arise at the single-neuron level through nonlinear synaptic integration mechanisms, at the network level through neural circuit interactions, or both. We analyzed supralinearity at the level of single cells, directly comparing EPSPs for both multiglomerular patterns and individual component sites. Multisite patterns often generated clear EPSPs even when input from any component site was negligible (Figure 7A), suggesting that supralinearity may arise intracortically via recurrent input from other PCx neurons directly driven by multisite patterns (Figure 3; see Haberly, 2001). Averaged data showed pattern-evoked EPSPs were consistently greater than the sum of components (Figures 7B and 7C; significant supralinearity in 5/6 neurons; $p < 0.05$, t-test). In addition, although the size of predicted EPSPs was typically minimal, multisite patterns reliably generated substantial synaptic input (Figure 7C), suggestive of substantial cortical amplification of weak MOB inputs. Together, our data reveal highly cooperative PCx responses to multiglomerular input, imparting strong sensitivity to combinatorial MOB activity that is the hallmark of sensory responses.

## Discussion

The initial representation of odor information in the brain is organized by the topographic map of OR input to the MOB. We used the OR map to assess the circuit mechanisms for odor processing in anterior PCx, which have remained enigmatic. Using *in vivo* photostimulation to drive highly defined patterns of cortical input, we found that individual PCx neurons fired in response to distinct patterns of coactive MOB glomeruli. Intracellular measurements revealed a distinct subset of relatively weak glomerular inputs to each cell. Together, the combination of network connectivity, synaptic strength, and cooperativity between glomerular inputs allows PCx neurons to detect specific patterns of MOB output, providing a mechanistic basis for cortical processing of complex odor stimuli.

### Cortical Decoding of Glomerular Combinations

Successive processing stages often represent increasingly complex features in the sensory environment (Hubel and Wiesel, 1959). What are the higher-order characteristics of chemical stimuli encoded in PCx? Virtually all odors comprise diverse chemical attributes that bind multiple ORs and drive distributed MOB activity patterns (Lin et al., 2006; Soucy et al., 2009). Several findings indicated that PCx neurons detect higher-order glomerular combinations embedded within such patterns. While single-glomerulus activation failed to generate PCx firing, firing appeared when several glomeruli were coactive (>3–4 uncaging sites, corresponding to ~6–10 glomeruli; Figure 3). Furthermore, responses of PCx neurons depended on the identity of activated glomeruli independent of total MOB output (Figure 4). Cortical decoding mechanisms thus appear to be matched the combinatorial quality of sensory-evoked MOB activity.

Is multiglomerular activity obligatory for cortical odor detection? Some odorants primarily activate a single OR type, such as those linked to specific anosmias (Keller et al., 2007). Some single M/T fibers generate large synaptic inputs *in vitro*, suggesting firing may require minimal summation in some cases (Apicella et al., 2010; Franks and Isaacson, 2006). While only multiglomerular patterns produced reliable PCx firing, single uncaging sites did generate spikes on occasional trials (Figure S2), suggesting combinatorial input may not be strictly essential. The PCx population may encompass a range of combination detection thresholds in order to balance sensitivity and feature combination. PCx responsiveness will likely be modulated by many factors, such as waking and arousal state (Murakami et al., 2005). Overall, however, our data indicate that detecting patterns of coactive glomeruli is a central neural computation in PCx (Apicella et al., 2010). It remains unclear how this principle will apply to odorants that evoke innate behavioral responses via the MOB (Kobayakawa et al., 2007; Lin et al., 2005). This will ultimately depend on whether such

behaviors are driven by single ORs or by distributed glomerular activity, and whether they are mediated through cortical pathways or by MOB projections to other brain regions such as the amygdala (Stowers and Logan, 2010).

## Synaptic Basis of Feature Combination in Single PCx Neurons

What are the neural circuit mechanisms for detecting specific multiglomerular patterns? Optical mapping of synaptic connections suggested that PCx neurons accomplish pattern detection at least in part through a connectivity rule where input to each PCx neuron is dominated by a specific subset of MOB glomeruli (Figure 6). Given weak single-glomerulus inputs, PCx neurons are predicted to fire when MOB activity patterns overlap with several of the glomeruli to which they are connected. Since each glomerulus encodes distinct physicochemical characteristics, direct feedforward activation of PCx neurons may thus explicitly encode collections of chemical attributes represented by their respective MOB glomeruli. Individual PCx cells thus combine several OR-based sensory channels in an initial step towards a unified neural representation of an odor object.

Different odors generate diverse MOB activity patterns, implying the PCx population must recognize many different glomerular combinations. Consistent with this, different PCx neurons received input from distinct sets of MOB glomeruli (Figure 6), and different cells responded to distinct uncaging patterns (Figure 4). The PCx population thus collectively samples a higher-dimensional space of glomerular combinations. Extrapolating from ~10% connectivity to ~2000 total glomeruli in the mouse (Soucy et al., 2009), one can estimate that each PCx neuron connects with ~200 glomeruli. The number of possible 200-glomerulus combinations is $>10^{500}$, which will be massively undersampled by the PCx population. Correspondingly, PCx firing was reliably triggered by MOB patterns with only 3-4 sites, suggesting cortical cells are not ‘grandmother’ neurons with highly specific input requirements. Instead, undersampling appears to be balanced by low-stringency coincidence detection requiring activity in a relatively small fraction of connected MOB glomeruli (Apicella et al., 2010; Franks and Isaacson, 2006). Our results are qualitatively consistent with recent monosynaptic tracing of PCx input (Miyamichi et al.), although we find substantially greater convergence of M/T input. Electrophysiological circuit mapping, besides revealing the functional strength of synaptic contacts, may allow detection of a greater proportion of MOB inputs.

Our experiments treat glomeruli as elementary processing units. *In vivo* imaging supports this assumption for presynaptic OR input (Wachowiak et al., 2004). Postsynaptically, each glomerulus contacts ~50–75 M/T neurons (Haberly, 1991), whose activity depends strongly on presynaptic OR input (Tan et al., 2010). However, all such ‘sister’ M/Ts do not necessarily respond identically (Dhawale et al., 2010; Egana et al., 2005; Fantana et al., 2008; Tan et al., 2010). Our data do not address whether sister M/Ts converge onto like cortical targets, although the small size of synaptic inputs suggested this was unlikely. Odor responses of second-order neurons are influenced by lateral interactions between glomeruli in both rat MOB (Fantana et al., 2008) and *Drosophila* antennal lobe (Olsen et al., 2007; Olsen and Wilson, 2008; Shang et al., 2007). While M/T responses were similar for single- and multi-site uncaging (Figure S3), any further decorrelation of odor-evoked firing by local MOB circuits may facilitate pattern separation by PCx. It also remains to be seen how PCx responses depend on temporal patterning of MOB output (Bathellier et al., 2008; Cury and Uchida, 2010; Dhawale et al., 2010; Kashiwadani et al., 1999; Schaefer and Margrie, 2007; Spors et al., 2006; Wesson et al., 2008; see Friedrich et al. [2004] and Perez-Orive et al. [2002]) for work in other species. Temporal decoding mechanisms have been described for both individual pyramidal neurons (Branco et al., 2010) and the PCx network (Stokes and Isaacson, 2010). While our experiments focused on circuit connectivity, in the future photostimulation may also help evaluate the role of timing in cortical processing.

### Cooperative Interactions Between Glomerular Inputs

Although glomerular pattern detection in PCx could potentially be explained by a simple linear feedforward mechanism, responses to coactive glomeruli were strongly supralinear. Besides receiving direct MOB input, PCx neurons form extensive recurrent interconnections with each other (Haberly and Bower, 1984; Haberly and Price, 1978; Johnson et al., 2000). It is currently unclear how feedforward and recurrent mechanisms interact during odor processing. Several factors implicated the intracortical circuit in generating supralinearity. Cooperativity appeared to emerge downstream of MOB, since M/T firing was similar for both single- and multi-site uncaging (Figure S3). Synaptic integration is largely linear in PCx pyramidal cells *in vitro* (Bathellier et al., 2009), arguing that cooperativity did not arise from nonlinear dendritic processing in single neurons (Larkum et al., 1999; Losonczy and Magee, 2006). Multiglomerular patterns generated robust EPSPs even when component sites did not generate detectable input, also pointing to an indirect source of synaptic input. Consistent with a recurrent source, uncaging stimuli that drove supralinear EPSPs also drove firing in PCx (≥3–4 uncaging sites; Figures 3 and 7). Together, these observations suggest that cortical odor processing consists not only of feedforward mechanisms, but also subsequent intracortical computations that remain poorly defined. Recurrent PCx connections are proposed to form an associative memory system that stores and recalls odor-specific patterns (Haberly, 2001; Haberly and Bower, 1984, 1989; Johnson et al., 2000; Wilson, 2009). Supralinear responses may reflect pattern completion by the associational network (Barnes et al., 2008; Wilson, 2009). Extracellular firing produced by multiglomerular stimuli likely reflected both direct MOB input and recurrent activity, which may have also contributed to the disparity between synaptic responses to single-site uncaging and odors (Figure 5). While further work will be needed to define the role of intracortical circuits, the robust cooperativity we found suggested they may contribute substantially to odor processing.

### Building Cortical Odor Representations

Our data may help explain some non-intuitive features of PCx sensory representations. Odors produce highly dispersed activity lacking apparent topography (Illig and Haberly, 2003; Rennaker et al., 2007; Stettler and Axel, 2009). Since M/T axons arborize widely throughout PCx with little or no spatial order (Buonviso et al., 1991; Nagayama et al., 2010; Ojima et al., 1984; Scott et al., 1980), specific combinations of direct MOB input may converge on postsynaptic cells at random positions, activating widely distributed neuronal populations. Activity may be further reconfigured by intracortical mechanisms, perhaps accounting for inconsistent responses to odor mixtures and their components (Stettler and Axel, 2009; Wilson, 2001). We rarely observed clear synaptic inhibition, which may be driven weakly if at all by single uncaging sites, or may be largely shunting at rest (Poo and Isaacson, 2009). While we focused on excitatory feedforward input from MOB, inhibition also figures prominently in PCx processing by limiting time windows for spiking and setting the timing of oscillatory firing (Kapur et al., 1997; Luna and Schoppa, 2008; Poo and Isaacson, 2009). The interplay between excitatory and inhibitory circuits in PCx is complex and dynamic (Stokes and Isaacson, 2010) and awaits further exploration.

Are there common cross-species principles for odor processing downstream of second-order neurons? In insects, the circuits that decode dense antennal lobe activity generate sparser and more selective odor representations in mushroom body (Perez-Orive et al., 2002; Turner et al., 2008). The ~10% glomerular connectivity we found is substantially lower than the ~50% connectivity between projection neurons and Kenyon cells in locust (Jortner et al., 2007), but is comparable to predictions in *Drosophila* (Turner et al., 2008). While it is currently unclear whether PCx representations are sparser or denser than in MOB in rodents, odors recruit substantial population activity in rodent PCx (Rennaker et al., 2007; Stettler

and Axel, 2009), and we observed PCx firing for a wide range of synthetic MOB patterns (Figure 3). In zebrafish, odors also evoke widespread population activity in higher-order olfactory centers, which is shaped considerably by local circuits (Nikonov and Caprio, 2007; Yaksi et al., 2009). Differences in higher-order odor representations across species may depend on both feedforward connectivity and the extent of local circuit processing.

The responses of PCx neurons to glomerular patterns likely reflected population activity states widely distributed across the cortical circuit (Rennaker et al., 2007; Stettler and Axel, 2009; Yaksi et al., 2009). Network-level cortical output states are unlikely to arise through feedforward mechanisms alone, but rather through a larger set of circuit computations that deserve additional investigation. Here, we describe the circuit logic that initially transmits information from MOB to anterior PCx. By revealing general principles for initial decoding of patterned MOB activity, our results provide a framework for circuit-based analysis of odor recognition and perception.

## Experimental Procedures

### Rodent Surgery and Electrophysiological Recordings

Mice were anesthetised with ketamine:dexdomitor for surgery, and transitioned to isoflurane or sevoflurane for neural recordings. The dorsal MOB was exposed via a small craniotomy and the dura carefully removed. All surgical procedures were in accordance with the guidelines of Duke University's Institutional Animal Care and Use Committee. Diagonal electrode penetrations targeting anterior PCx were made through a second posterior craniotomy. Extracellular spikes were recorded with tungsten microelectrodes (2-4 MΩ) and amplified 10,000X (A-M Systems Model 1800). Intracellular recordings were made with sharp electrodes (1.0 X 0.5 mm borosilicate glass; resistance 70–120 MΩ, 3M K-acetate) and an Axoclamp 2B amplifier (Molecular Devices). See Supplemental Experimental Procedures for additional details.

### Odor Stimulation

Our test panel contained 13 odorants: propionic acid, isobutyraldehyde, geraniol, methyl salicylate, guaiacol, citral, (+)-carvone, 2-pentyl furan, 1-pentanol, diethylamine, eugenol, amyl acetate, and limonene (Sigma). Compounds were diluted in mineral oil to give a 50 ppm headspace concentration, and further diluted 1:10 in the flow stream. Odors were presented for 3–4 seconds, controlled with solenoid valves. See Supplemental Experimental Procedures for additional details.

### Glutamate Uncaging

The dorsal MOB was superfused with 1.5-2 mM MNI-caged glutamate (Tocris) in ACSF, exchanged after each uncaging trial. UV pulses (355nm, 0.5–0.6 ms, ~40μm diameter, ~40 mW) were scanned across the MOB in an 8x12 grid with 100μm spacing, using a custom scan system and control software. Multisite uncaging stimuli were generated by randomly selecting scan grid positions in nonoverlapping patterns, generating patterns similar to odor-evoked glomerular activity. Patterns were delivered quasisimultaneously by switching scan positions every 1 ms (Figure S3). See Supplemental Experimental Procedures for additional details.

### Data Acquisition and Analysis

Electrophysiological data were acquired with Spike2 software and Power 1401 digitizer (CED) or with custom routines and hardware (Igor Pro and PCI-6035E, National Instruments). Firing rates and intracellular membrane potential were averaged over uncaging trials, or over respiratory cycles during odor presentation. Uncaging responses were

evaluated in a 150 ms window. Photostimulation response maps were constructed based the size of evoked responses at each scan grid location. See Supplemental Experimental Procedures for additional details.

## Supplementary Material

Refer to Web version on PubMed Central for supplementary material.

## Acknowledgments

We thank V. Bhandawat, D. Fitzpatrick, J. Hernandez, S. Van Hooser, and members of the Ehlers lab for comments on the manuscript. We dedicate this manuscript to the memory of Larry Katz, whose scientific vision and technical innovations laid the groundwork for this study. This work was supported by NIH grant R01 MH086339 and the Howard Hughes Medical Institute (to M.D.E.).

## References

Apicella A, Yuan Q, Scanziani M, Isaacson JS. Pyramidal cells in piriform cortex receive convergent input from distinct olfactory bulb glomeruli. J Neurosci. 2010; 30:14255–14260. [PubMed: 20962246]

Araneda RC, Kini AD, Firestein S. The molecular receptive range of an odorant receptor. Nat Neurosci. 2000; 3:1248–1255. [PubMed: 11100145]

Arenkiel BR, Peca J, Davison IG, Feliciano C, Deisseroth K, Augustine GJ, Ehlers MD, Feng G. In vivo light-induced activation of neural circuitry in transgenic mice expressing channelrhodopsin-2. Neuron. 2007; 54:205–218. [PubMed: 17442243]

Arevian AC, Kapoor V, Urban NN. Activity-dependent gating of lateral inhibition in the mouse olfactory bulb. Nat Neurosci. 2008; 11:80–87. [PubMed: 18084286]

Barnes DC, Hofacer RD, Zaman AR, Rennaker RL, Wilson DA. Olfactory perceptual stability and discrimination. Nat Neurosci. 2008; 11:1378–1380. [PubMed: 18978781]

Bathellier B, Buhl DL, Accolla R, Carleton A. Dynamic ensemble odor coding in the mammalian olfactory bulb: sensory information at different timescales. Neuron. 2008; 57:586–598. [PubMed: 18304487]

Bathellier B, Margrie TW, Larkum ME. Properties of piriform cortex pyramidal cell dendrites: implications for olfactory circuit design. J Neurosci. 2009; 29:12641–12652. [PubMed: 19812339]

Bozza T, Feinstein P, Zheng C, Mombaerts P. Odorant receptor expression defines functional units in the mouse olfactory system. J Neurosci. 2002; 22:3033–3043. [PubMed: 11943806]

Branco T, Clark BA, Hausser M. Dendritic Discrimination of Temporal Input Sequences in Cortical Neurons. Science. 2010

Buonviso N, Revial MF, Jourdan F. The Projections of Mitral Cells from Small Local Regions of the Olfactory Bulb: An Anterograde Tracing Study Using PHA-L (Phaseolus vulgaris Leucoagglutinin). Eur J Neurosci. 1991; 3:493–500. [PubMed: 12106481]

Callaway EM, Katz LC. Photostimulation using caged glutamate reveals functional circuitry in living brain slices. Proc Natl Acad Sci U S A. 1993; 90:7661–7665. [PubMed: 7689225]

Cury KM, Uchida N. Robust odor coding via inhalation-coupled transient activity in the mammalian olfactory bulb. Neuron. 2010; 68:570–585. [PubMed: 21040855]

Dhawale AK, Hagiwara A, Bhalla US, Murthy VN, Albeanu DF. Non-redundant odor coding by sister mitral cells revealed by light addressable glomeruli in the mouse. Nat Neurosci. 2010

Egana JI, Aylwin ML, Maldonado PE. Odor response properties of neighboring mitral/tufted cells in the rat olfactory bulb. Neuroscience. 2005; 134:1069–1080. [PubMed: 15994017]

Fantana AL, Soucy ER, Meister M. Rat olfactory bulb mitral cells receive sparse glomerular inputs. Neuron. 2008; 59:802–814. [PubMed: 18786363]

Franks KM, Isaacson JS. Synapse-specific downregulation of NMDA receptors by early experience: a critical period for plasticity of sensory input to olfactory cortex. Neuron. 2005; 47:101–114. [PubMed: 15996551]

Franks KM, Isaacson JS. Strong single-fiber sensory inputs to olfactory cortex: implications for olfactory coding. Neuron. 2006; 49:357–363. [PubMed: 16446140]

Friedrich RW, Habermann CJ, Laurent G. Multiplexing using synchrony in the zebrafish olfactory bulb. Nat Neurosci. 2004; 7:862–871. [PubMed: 15273692]

Gottfried JA. Central mechanisms of odour object perception. Nat Rev Neurosci. 2010; 11:628–641. [PubMed: 20700142]

Haberly, LB. Olfactory Cortex. In: Shepherd, GM., editor. Synaptic Organization of the Brain. New York: Oxford University Press; 1991. p. 317-345.

Haberly LB. Parallel-distributed processing in olfactory cortex: new insights from morphological and physiological analysis of neuronal circuitry. Chem Senses. 2001; 26:551–576. [PubMed: 11418502]

Haberly LB, Bower JM. Analysis of association fiber system in piriform cortex with intracellular recording and staining techniques. J Neurophysiol. 1984; 51:90–112. [PubMed: 6319624]

Haberly LB, Bower JM. Olfactory cortex: model circuit for study of associative memory? Trends Neurosci. 1989; 12:258–264. [PubMed: 2475938]

Haberly LB, Price JL. Association and commissural fiber systems of the olfactory cortex of the rat. J Comp Neurol. 1978; 178:711–740. [PubMed: 632378]

Haddad R, Lapid H, Harel D, Sobel N. Measuring smells. Curr Opin Neurobiol. 2008; 18:438–444. [PubMed: 18824102]

Hubel DH, Wiesel TN. Receptive fields of single neurones in the cat's striate cortex. J Physiol. 1959; 148:574–591. [PubMed: 14403679]

Illig KR, Haberly LB. Odor-evoked activity is spatially distributed in piriform cortex. J Comp Neurol. 2003; 457:361–373. [PubMed: 12561076]

Jacob V, Le Cam J, Ego-Stengel V, Shulz DE. Emergent properties of tactile scenes selectively activate barrel cortex neurons. Neuron. 2008; 60:1112–1125. [PubMed: 19109915]

Johnson DM, Illig KR, Behan M, Haberly LB. New features of connectivity in piriform cortex visualized by intracellular injection of pyramidal cells suggest that "primary" olfactory cortex functions like "association" cortex in other sensory systems. J Neurosci. 2000; 20:6974–6982. [PubMed: 10995842]

Jortner RA, Farivar SS, Laurent G. A simple connectivity scheme for sparse coding in an olfactory system. J Neurosci. 2007; 27:1659–1669. [PubMed: 17301174]

Kapur A, Pearce RA, Lytton WW, Haberly LB. GABAA-mediated IPSCs in piriform cortex have fast and slow components with different properties and locations on pyramidal cells. J Neurophysiol. 1997; 78:2531–2545. [PubMed: 9356403]

Kashiwadani H, Sasaki YF, Uchida N, Mori K. Synchronized oscillatory discharges of mitral/tufted cells with different molecular receptive ranges in the rabbit olfactory bulb. J Neurophysiol. 1999; 82:1786–1792. [PubMed: 10515968]

Katada S, Hirokawa T, Oka Y, Suwa M, Touhara K. Structural basis for a broad but selective ligand spectrum of a mouse olfactory receptor: mapping the odorant-binding site. J Neurosci. 2005; 25:1806–1815. [PubMed: 15716417]

Keller A, Zhuang H, Chi Q, Vosshall LB, Matsunami H. Genetic variation in a human odorant receptor alters odour perception. Nature. 2007; 449:468–472. [PubMed: 17873857]

Kobayakawa K, Kobayakawa R, Matsumoto H, Oka Y, Imai T, Ikawa M, Okabe M, Ikeda T, Itohara S, Kikusui T, et al. Innate versus learned odour processing in the mouse olfactory bulb. Nature. 2007; 450:503–508. [PubMed: 17989651]

Larkum ME, Zhu JJ, Sakmann B. A new cellular mechanism for coupling inputs arriving at different cortical layers. Nature. 1999; 398:338–341. [PubMed: 10192334]

Lei H, Mooney R, Katz LC. Synaptic integration of olfactory information in mouse anterior olfactory nucleus. J Neurosci. 2006; 26:12023–12032. [PubMed: 17108176]

Lin DY, Shea SD, Katz LC. Representation of natural stimuli in the rodent main olfactory bulb. Neuron. 2006; 50:937–949. [PubMed: 16772174]

Lin DY, Zhang SZ, Block E, Katz LC. Encoding social signals in the mouse main olfactory bulb. Nature. 2005; 434:470–477. [PubMed: 15724148]

Livermore A, Laing DG. Influence of training and experience on the perception of multicomponent odor mixtures. J Exp Psychol Hum Percept Perform. 1996; 22:267–277. [PubMed: 8934843]

Losonczy A, Magee JC. Integrative properties of radial oblique dendrites in hippocampal CA1 pyramidal neurons. Neuron. 2006; 50:291–307. [PubMed: 16630839]

Luna VM, Schoppa NE. GABAergic circuits control input-spike coupling in the piriform cortex. J Neurosci. 2008; 28:8851–8859. [PubMed: 18753387]

Malnic B, Hirono J, Sato T, Buck LB. Combinatorial receptor codes for odors. Cell. 1999; 96:713–723. [PubMed: 10089886]

Miyamichi K, Amat F, Moussavi F, Wang C, Wickersham I, Wall NR, Taniguchi H, Tasic B, Huang ZJ, He Z, et al. Cortical representations of olfactory input by trans-synaptic tracing. Nature.

Mombaerts P, Wang F, Dulac C, Chao SK, Nemes A, Mendelsohn M, Edmondson J, Axel R. Visualizing an olfactory sensory map. Cell. 1996; 87:675–686. [PubMed: 8929536]

Mori K, Nagao H, Yoshihara Y. The olfactory bulb: coding and processing of odor molecule information. Science. 1999; 286:711–715. [PubMed: 10531048]

Murakami M, Kashiwadani H, Kirino Y, Mori K. State-dependent sensory gating in olfactory cortex. Neuron. 2005; 46:285–296. [PubMed: 15848806]

Nagayama S, Enerva A, Fletcher ML, Masurkar AV, Igarashi KM, Mori K, Chen WR. Differential axonal projection of mitral and tufted cells in the mouse main olfactory system. Front Neural Circuits. 2010:4. [PubMed: 20300468]

Nikonov AA, Caprio J. Responses of olfactory forebrain units to amino acids in the channel catfish. J Neurophysiol. 2007; 97:2490–2498. [PubMed: 17251362]

Ojima H, Mori K, Kishi K. The trajectory of mitral cell axons in the rabbit olfactory cortex revealed by intracellular HRP injection. J Comp Neurol. 1984; 230:77–87. [PubMed: 6096415]

Olsen SR, Bhandawat V, Wilson RI. Excitatory interactions between olfactory processing channels in the Drosophila antennal lobe. Neuron. 2007; 54:89–103. [PubMed: 17408580]

Olsen SR, Wilson RI. Lateral presynaptic inhibition mediates gain control in an olfactory circuit. Nature. 2008; 452:956–960. [PubMed: 18344978]

Perez-Orive J, Mazor O, Turner GC, Cassenaer S, Wilson RI, Laurent G. Oscillations and sparsening of odor representations in the mushroom body. Science. 2002; 297:359–365. [PubMed: 12130775]

Poo C, Isaacson JS. Odor representations in olfactory cortex: "sparse" coding, global inhibition, and oscillations. Neuron. 2009; 62:850–861. [PubMed: 19555653]

Reid RC, Alonso JM. Specificity of monosynaptic connections from thalamus to visual cortex. Nature. 1995; 378:281–284. [PubMed: 7477347]

Rennaker RL, Chen CF, Ruyle AM, Sloan AM, Wilson DA. Spatial and temporal distribution of odorant-evoked activity in the piriform cortex. J Neurosci. 2007; 27:1534–1542. [PubMed: 17301162]

Root CM, Masuyama K, Green DS, Enell LE, Nassel DR, Lee CH, Wang JW. A presynaptic gain control mechanism fine-tunes olfactory behavior. Neuron. 2008; 59:311–321. [PubMed: 18667158]

Rubin BD, Katz LC. Optical imaging of odorant representations in the mammalian olfactory bulb. Neuron. 1999; 23:499–511. [PubMed: 10433262]

Schaefer AT, Margrie TW. Spatiotemporal representations in the olfactory system. Trends Neurosci. 2007; 30:92–100. [PubMed: 17224191]

Scott JW, McBride RL, Schneider SP. The organization of projections from the olfactory bulb to the piriform cortex and olfactory tubercle in the rat. J Comp Neurol. 1980; 194:519–534. [PubMed: 7451680]

Serizawa S, Miyamichi K, Nakatani H, Suzuki M, Saito M, Yoshihara Y, Sakano H. Negative feedback regulation ensures the one receptor-one olfactory neuron rule in mouse. Science. 2003; 302:2088–2094. [PubMed: 14593185]

Shang Y, Claridge-Chang A, Sjulson L, Pypaert M, Miesenbock G. Excitatory local circuits and their implications for olfactory processing in the fly antennal lobe. Cell. 2007; 128:601–612. [PubMed: 17289577]

Shepherd GM, Pologruto TA, Svoboda K. Circuit analysis of experience-dependent plasticity in the developing rat barrel cortex. Neuron. 2003; 38:277–289. [PubMed: 12718861]

Soucy ER, Albeanu DF, Fantana AL, Murthy VN, Meister M. Precision and diversity in an odor map on the olfactory bulb. Nat Neurosci. 2009; 12:210–220. [PubMed: 19151709]

Spors H, Wachowiak M, Cohen LB, Friedrich RW. Temporal dynamics and latency patterns of receptor neuron input to the olfactory bulb. J Neurosci. 2006; 26:1247–1259. [PubMed: 16436612]

Stettler DD, Axel R. Representations of odor in the piriform cortex. Neuron. 2009; 63:854–864. [PubMed: 19778513]

Stokes CC, Isaacson JS. From dendrite to soma: dynamic routing of inhibition by complementary interneuron microcircuits in olfactory cortex. Neuron. 2010; 67:452–465. [PubMed: 20696382]

Stowers L, Logan DW. Olfactory mechanisms of stereotyped behavior: on the scent of specialized circuits. Curr Opin Neurobiol. 2010; 20:274–280. [PubMed: 20338743]

Tan J, Savigner A, Ma W, Luo M. Odor Information Processing by the Olfactory Bulb Analyzed in Gene-Targeted Mice. Neuron. 2010; 65:912–926. [PubMed: 20346765]

Turner GC, Bazhenov M, Laurent G. Olfactory representations by Drosophila mushroom body neurons. J Neurophysiol. 2008; 99:734–746. [PubMed: 18094099]

Uchida N, Takahashi YK, Tanifuji M, Mori K. Odor maps in the mammalian olfactory bulb: domain organization and odorant structural features. Nat Neurosci. 2000; 3:1035–1043. [PubMed: 11017177]

Usrey WM, Alonso JM, Reid RC. Synaptic interactions between thalamic inputs to simple cells in cat visual cortex. J Neurosci. 2000; 20:5461–5467. [PubMed: 10884329]

Wachowiak M, Cohen LB. Representation of odorants by receptor neuron input to the mouse olfactory bulb. Neuron. 2001; 32:723–735. [PubMed: 11719211]

Wachowiak M, Denk W, Friedrich RW. Functional organization of sensory input to the olfactory bulb glomerulus analyzed by two-photon calcium imaging. Proc Natl Acad Sci U S A. 2004; 101:9097–9102. [PubMed: 15184670]

Wesson DW, Carey RM, Verhagen JV, Wachowiak M. Rapid encoding and perception of novel odors in the rat. PLoS Biol. 2008; 6:e82. [PubMed: 18399719]

Wilson DA. Comparison of odor receptive field plasticity in the rat olfactory bulb and anterior piriform cortex. J Neurophysiol. 2000; 84:3036–3042. [PubMed: 11110830]

Wilson DA. Receptive fields in the rat piriform cortex. Chem Senses. 2001; 26:577–584. [PubMed: 11418503]

Wilson DA. Pattern separation and completion in olfaction. Ann N Y Acad Sci. 2009; 1170:306–312. [PubMed: 19686152]

Wilson DA, Stevenson RJ. The fundamental role of memory in olfactory perception. Trends Neurosci. 2003; 26:243–247. [PubMed: 12744840]

Wilson RI, Mainen ZF. Early events in olfactory processing. Annu Rev Neurosci. 2006; 29:163–201. [PubMed: 16776583]

Yaksi E, von Saint Paul F, Niessing J, Bundschuh ST, Friedrich RW. Transformation of odor representations in target areas of the olfactory bulb. Nat Neurosci. 2009; 12:474–482. [PubMed: 19305401]

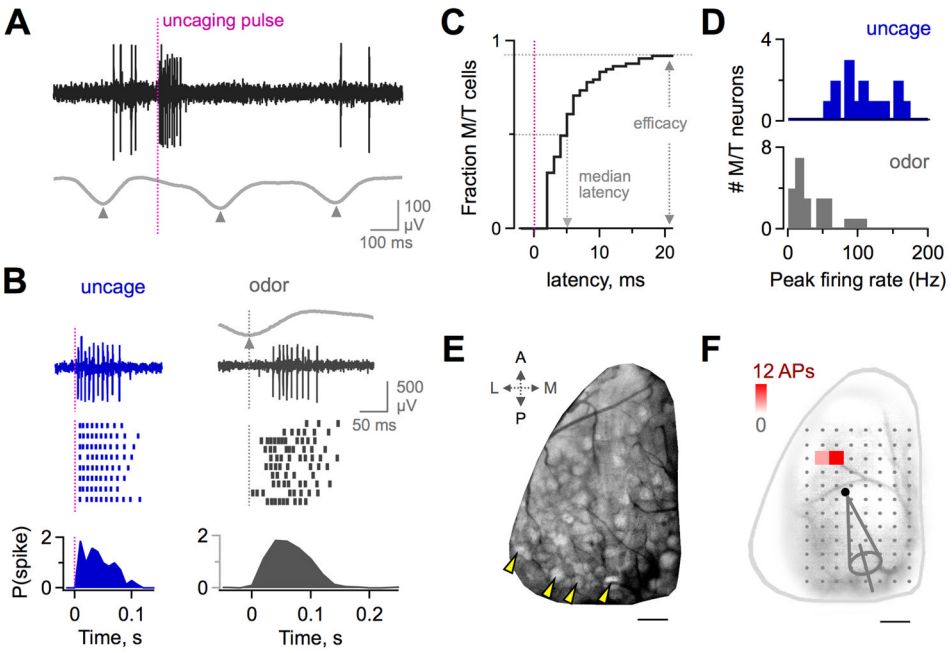


**Figure 1. MOB Photostimulation Drives Robust M/T Firing *In Vivo***

(A) Extracellular recording of M/T action potential firing produced by uncaging (black), generated between resting activity coupled to respiration (gray; triangles show inspiration). Vertical line indicates uncaging pulse.

(B) Uncaging reliably produces high-frequency M/T firing (left, blue) comparable to robust odor responses (right, gray). Top, raw traces from a single trial (uncaging) or respiratory cycle (odors). Middle, rasters from successive trials or inhalations. Bottom, PSTH of mean spike count in 10 ms bins.

(C) Cumulative plot of latency to first photostimulated M/T spikes. Firing occurs with high efficacy and at short latency (>90% of M/Ts, horizontal dashed line; median latency ~5 ms).

(D) Comparison of peak M/T firing rates for uncaging (blue) and odorants (gray). Data show most effective uncaging sites or odorants for each neuron.

(E) Image of the OR map in the dorsal MOB from a mouse line with fluorescently labeling of axon terminals of sensory neurons. Arrowheads denote individual glomeruli. Scale bar, 200 µm.

(F) Map of spike output from a single M/T generated by *in vivo* scanning photostimulation of the dorsal MOB. Color indicates the mean spike count at each location; dots indicate ineffective sites (100 ms analysis window). Pipette shows recording location in the M/T layer. Scale bar, 200 µm. See also Figure S1.

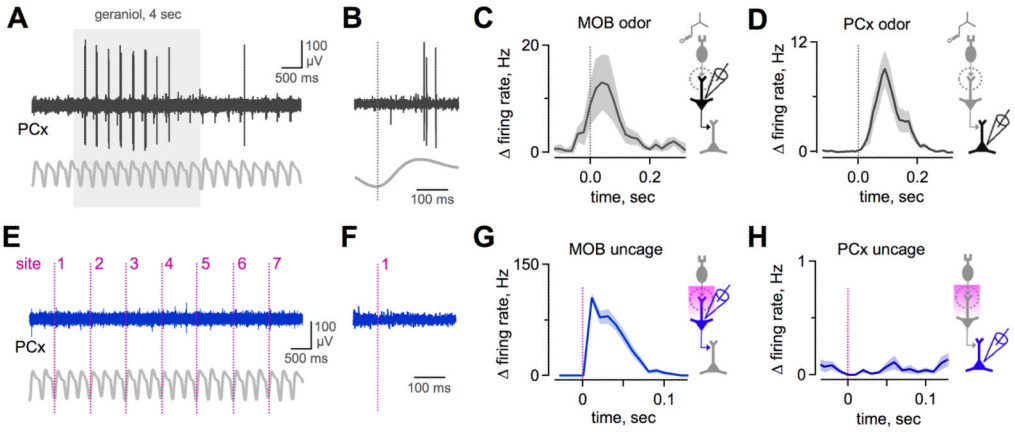


**Figure 2. PCx Neurons Are Insensitive to Single-Glomerulus Activation**

(A) Odor-evoked response in a PCx neuron. Shaded box, odor delivery. Gray trace, respiration.

(B) Expanded view from (A) showing firing during a single inhalation. Vertical line, inspiration peak.

(C) Mean change in odor-evoked firing rate averaged across all M/Ts, aligned to inspiration peak (vertical line). Data show most effective odorant for each neuron (25 cells, 13 odorants/cell).

(D) Mean odor-evoked activity of PCx neurons averaged across all odors and cells. (23 cells, 4–13 odorants/cell).

(E) In the same odor-responsive PCx neuron shown in (A), uncaging at single MOB locations generated no firing. Vertical lines indicate uncaging pulses at various scan grid locations (7/96 shown).

(F) Expanded view from (E). Individual MOB sites were consistently ineffective at driving PCx firing over several repeated uncaging trials.

(G) Mean change in M/T firing rate produced by single-site uncaging in MOB, calculated for each cell's most effective uncaging site (n = 26 cells).

(H) Mean change in PCx firing rate for single-site uncaging (n = 31 cells; note expanded scale relative to [D] and [G]). Despite robust M/T activation, PCx neurons were consistently unresponsive. See also Figure S2.

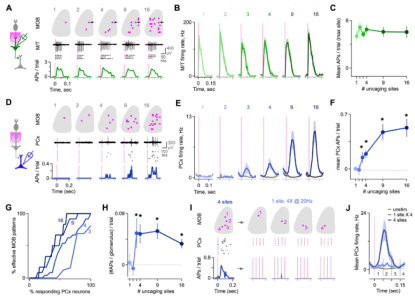

**Figure 3. PCx Firing Emerges When Multiple Glomeruli Are Coactive**

(A) Example M/T neuron in MOB tested with a series of multisite patterns encompassing increasing numbers of glomeruli. M/T responses were independent of pattern size. Traces, raw single-trial data. Rasters, repeated presentations. Histograms, spike probability in 10 ms bins. See also Figure S3.

(B) Mean firing rates for all M/Ts tested with multisite patterns, quantified for the most effective individual site (1, left) and for the set of patterns containing this site (2–16, right; n = 11 cells).

(C) Mean M/T spike count is independent of number of uncaging sites in the stimulus pattern (n = 11 cells).

(D) Example PCx neuron tested with a series of multisite patterns. Firing emerged only when several glomeruli were coactive.

(E) Mean firing rates for all PCx neurons in response to patterns of increasing size. Spiking appeared only when patterns contained ≥3–4 sites (n = 14 – 53 cells for various pattern sizes).

(F) PCx input-output function showing the dependence of firing on the number of MOB uncaging sites. Asterisks show significant difference relative to rest ($p < 0.05$, t-test; n = 14 – 53 cells).

(G) Cumulative plot of PCx neuron activation with additional MOB uncaging sites. For 3-site stimuli (light blue), most cells were unresponsive or driven by a small set of patterns (left), while a few cells responded to many patterns (right). For stimuli with additional sites (darker blue traces, indicated by number labels), a greater proportion of cells was activated, and cells reponded to a greater fraction of patterns.

(H) Mean PCx spike count for different sized patterns, divided by number of uncaging sites to normalize for total cortical input. The ‘per glomerulus’ contribution rose steeply for patterns of 3 or more sites.

(I) Comparison of PCx responses to composite patterns and component sites. For an effective 4-site pattern, there was little or no response to individual sites stimulated 4 times at 20 Hz.

(J) Population analysis shows patterns are consistently more effective than repeated stimulation of components (n = 10 cells). Dark blue, mean firing rate for effective 4-site stimuli. Light blue, firing for component sites activated 4 times at 20Hz. Gray, resting activity. Vertical lines, uncaging pulses.

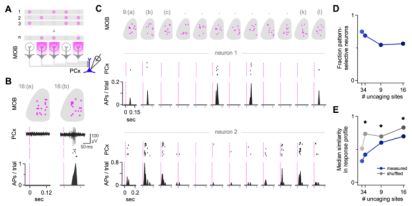

**Figure 4. PCx Neurons Detect Specific Patterns of Coactive Glomeruli**

(A) Experimental schematic. PCx firing was recorded extracellularly while photoactivating the same number of MOB glomeruli in different combinations.

(B) Example PCx neuron that was unresponsive to one multiglomerular MOB pattern (left), but reliably activated by another (right). Top, MOB uncaging patterns. Middle, PCx responses on a single trial (trace) and repeated presentations (rasters). Bottom, histogram of spike probability in 10 ms bins.

(C) Two additional PCx neurons tested with a series of 9-site uncaging stimuli that drove non-overlapping glomerular activity patterns. Data shown as in (B). Only a select subset of patterns consistently evoked firing in each neuron, and each cell responded to a different subset of patterns. Neurons were recorded in different experimental animals.

(D) Over half of PCx neurons had significant pattern-selective responses compared to randomly shuffled data ($p < 0.05$; 10,000 iterations).

(E) Different PCx neurons consistently responded to different MOB patterns. Median similarity between the set of patterns activating each cell was consistently lower for measured (blue circles) than for shuffled data (gray circles). See also Figure S4.

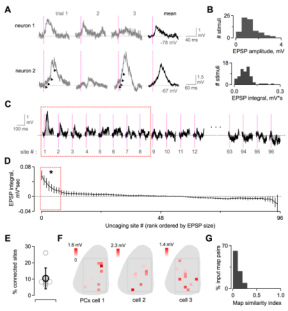

**Figure 5. Intracellular Recordings Reveal Weak Input to PCx Neurons From Distinct Subpopulations of MOB Glomeruli**

(A) Synaptic input generated by single-site optical microstimulation of MOB, shown for two example PCx neurons. EPSPs were typically 0.5–2.5 mV in amplitude. Gray, single trials. Black, averaged response. Smaller individual inputs were often apparent within compound EPSPs (arrowheads), presumably reflecting M/T spike trains. Vertical lines, uncaging pulses.

(B) Distribution of EPSP sizes for all MOB sites classified as synaptically connected. Top, EPSP amplitudes. Bottom, EPSP integrals.

(C) Cortical EPSPs generated by single-site MOB photostimulation mapping, shown rank-ordered by size at each scan location. Red box indicates sites classified as synaptically connected (see Experimental Procedures). Vertical lines, UV pulse. Gray shading, integrated EPSP area.

(D) Rank-ordered distribution of EPSPs for all scan locations, averaged across all PCx neurons (mean EPSP integral ± SEM; n = 8 cells). Synaptic input was consistently dominated by a small fraction of sites independent of their classification as synaptically connected (8 sites significantly different from resting activity, enclosed by red box; $p < 0.05$; t-test).

(E) PCx neurons were connected on average to 10.5 ± 6.4% of tested MOB locations. Gray circles, data for single neurons. Black, population average (mean ± SEM, n = 8 neurons).

(F) Glomerular input maps for three example PCx neurons showing the dispersed MOB locations producing detectable synaptic input. Color scale shows EPSP amplitudes at each connected site. Leftmost map corresponds to (A); cells were recorded in different animals.

(G) Input maps for different PCx neurons were consistently dissimilar. Plot shows correlation coefficients for all pairwise comparisons between maps for all neurons, after converting each map to a binary vector.

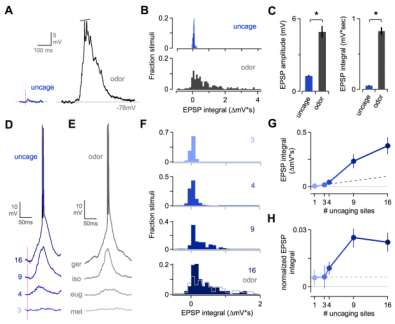

**Figure 6. Coactive MOB Glomeruli Generate Supralinear Synaptic Responses in PCx Neurons**

(A) Comparison of EPSPs for single-site uncaging (left, blue) and odorant stimulation (right, gray) in the same PCx neuron. Trace shows a single respiratory cycle; spikes have been truncated.

(B) Distribution of EPSPs compared for single-site photostimulation mapping (top, blue) and odorants (bottom, gray). Data shows responses for connected uncaging sites (71/768 locations, 8 cells x 96 MOB sites); all odor responses were included regardless of size (9 cells x 13 odorants).

(C) Mean EPSPs are many times larger for odors than for single uncaging sites, indicating single-glomerulus inputs are insufficient to account for sensory responses. Left and right plots show EPSP amplitude and integral respectively. Mean amplitudes ± SEM are 1.3 ± 0.1 and 4.9 mV ± 0.5 for uncaging and odors respectively, $p \ll 0.01$; mean integrals, 0.052 ± 0.008 mV*sec and 0.826 ± 0.056 mV*sec, $p \ll 0.01$.

(D) Example PCx neuron showing synaptic responses to uncaging patterns of increasingly larger size, indicated to the left of each trace. Larger patterns consistently generated EPSPs 10–20 mV in size. Vertical line, uncaging pulse.

(E) EPSPs evoked by various odorants in another PCx neuron. Synaptic responses to multisite uncaging and sensory stimuli were comparable. Traces show one respiratory cycle during odor presentation. Ger, geraniol; iso, isobutyraldehyde; eug, eugenol; met, methyl salicylate.

(F) Distribution of EPSP sizes for uncaging patterns of increasing size, indicated on each panel. Data for odor-evoked EPSPs is replotted from (B) and overlaid on the 16-site data for comparison (bottom panel, gray line).

(G) Multisite MOB patterns generate a supralinear increase in PCx synaptic responses. Dashed line shows the increase predicted by simple linear summation of single-site input.

(H) Synaptic responses to multisite patterns as in (G), normalized by dividing each uncaging-evoked EPSP by the number of MOB sites. Patterns containing ≥4 sites generated a ‘per-glomerulus’ PCx response that increased sharply above the constant per-site relationship predicted by linear summation (dashed line).

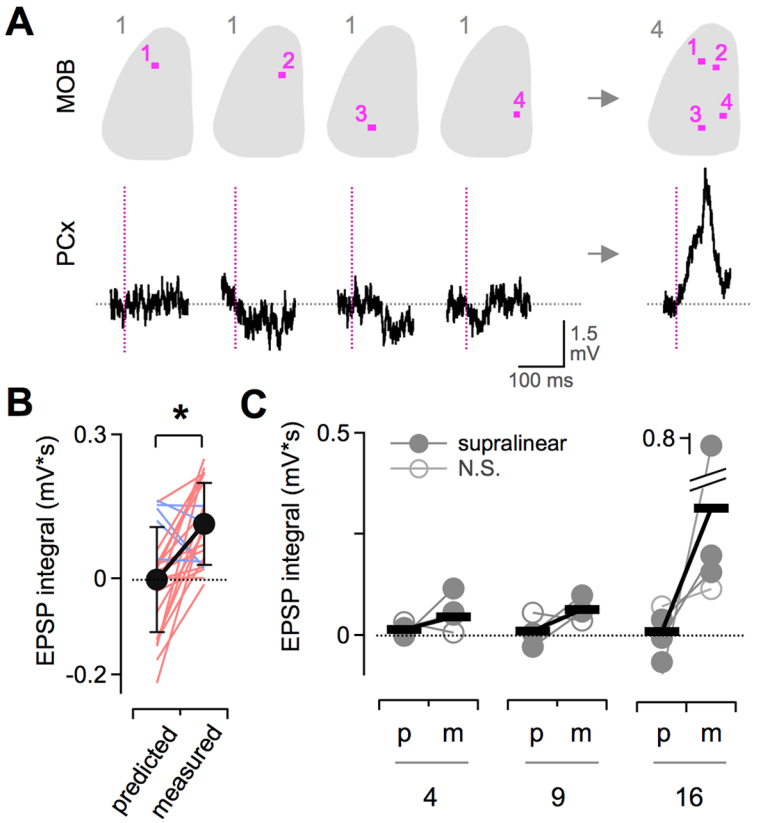


**Figure 7. Cooperative Responses in Single PCx Neurons**

(A) Direct comparison of EPSPs for multisite patterns and individual component sites in the same PCx neuron. Example shows a substantial EPSP for a 4-site stimulus (right) even in the absence of measurable input from any single component site (left). Top, MOB uncaging patterns. Bottom, PCx neuron membrane potential. Vertical lines, uncaging pulse.

(B) Full set of EPSPs for all 4-site patterns and their components for the cell shown in (A). Measured responses to patterns were consistently larger than predicted by linear summation of component sites ($p < 0.01$; 24 measured/predicted comparisons; red and blue indicate supra- and sub-linearity respectively).

(C) Supralinear summation across the PCx population. Predicted (p) and measured (m) synaptic responses for each single neuron are shown as connected circles, averaged across all patterns as in (B). Horizontal bars show mean values for all cells. 5/6 neurons displayed significant supralinearity for one or more set of multisite (filled circles; $p < 0.05$, t-test; N.S., non-significant pairs).